water

MDPI

Article

Algal Decomposition Accelerates Denitrification as Evidenced by the High-Resolution Distribution of Nitrogen Fractions in the Sediment–Water Interface of Eutrophic Lakes

Yu Yao [1,2,3,†], Ying Chen [1,2,3,†], Ruiming Han [1,2,3,*], Desheng Chen [1,2,3], Huanxin Ma [1,2,3], Xiaoxiang Han [1,2,3], Yuqi Feng [1,2,3] and Chenfei Shi [1,2,3]

[1] School of Environment, Nanjing Normal University, Nanjing 210023, China; yaoyu@njnu.edu.cn (Y.Y.)
[2] Jiangsu Center for Collaborative Innovation in Geographical Information Resource Development and Application, Nanjing 210023, China
[3] Jiangsu Engineering Laboratory of Water and Soil Eco-Remediation, Nanjing Normal University, Nanjing 210023, China
* Correspondence: 09386@njnu.edu.cn; Tel./Fax: +86-025-8378-7332
† These authors contributed equally to this work.

Abstract: This study investigates the decomposition process of algal blooms (ABs) in eutrophic lakes and its impact on the labile endogenous nitrogen (N) cycle. In situ techniques such as diffusive gradients in thin films (DGT) and high-resolution dialysis (HR-Peeper) were employed to decipher the vertical distribution of N fractions within the sediment–water interface (SWI) in Taihu, China. Additionally, an annular flume was used to simulate regional differences in lake conditions and understand labile nitrogen transformation during AB decomposition. This study reveals that the NH_4^+-N fraction exuded from algae is subsequently converted into NO_3-N and NO_2-N through nitrification, resulting in a significant increase in the concentrations of NO_3^--N and NO_2^--N at the SWI. The decomposition of algae also induces a significant increase in dissolved organic matter (DOM) concentration, referring to humic acid and humus-like components; a seven-millimeter decrease in dissolved oxygen (DO) penetration depth; as well as a significant decrease in the pH value near the SWI, which consequently promotes denitrification processes in the sediment. Moreover, the decomposition process influences nitrogen distribution patterns and the role conversion of sediments between a "source" and a "sink" of nitrogen. This investigation provides evidence on the migration and/or transformation of N fractions and offers insights into the dynamic processes across the SWI in eutrophic lakes.

Keywords: nitrogen; algal decomposition; high-resolution; sediment–water interface; eutrophic lake

Citation: Yao, Y.; Chen, Y.; Han, R.; Chen, D.; Ma, H.; Han, X.; Feng, Y.; Shi, C. Algal Decomposition Accelerates Denitrification as Evidenced by the High-Resolution Distribution of Nitrogen Fractions in the Sediment–Water Interface of Eutrophic Lakes. *Water* **2024**, *16*, 341. https://doi.org/10.3390/w16020341

Academic Editor: Christos S. Akratos

Received: 9 October 2023
Revised: 14 November 2023
Accepted: 12 January 2024
Published: 19 January 2024

1. Introduction

An overload of exogenous nitrogen element input has increased eutrophication and the formation of algal blooms (ABs) in aquatic ecosystems over the world [1–5]. Numerous ABs have directly impacted the ecological and economic sustainability of lakes, contaminated drinking water sources, and consequently threated human health [6–8]. Labile nitrogen (LN) fractions could promote eutrophication and AB occurrence in aquatic ecosystems [9–11]. The algal decomposition process leads to variations in the physicochemical properties of the microenvironment of the sediment–water interface (SWI) [12], accelerating N release from sediment to the overlying water, which contributes to the further cumulative increase in algal biomass in the long term [13]. Thus, a comprehensive understanding of the dynamics of labile N fractions under the influence of algal decomposition is required to take measures to manage and protect freshwater resources.

Numerous investigations have indicated that the decomposition of harmful algal blooms (HABs) might significantly influence the N dynamics in freshwater ecosystems.

Cyanobacteria have high uptake affinity and excellent storage capacity for dissolved inorganic nitrogen (DIN), while organic N-containing components such as urea, amino acids, nucleic acid, and polypeptide derived from dissolved organic nitrogen (DON) also contribute remarkably to the proliferation of cyanobacteria. Moreover, the photosynthesis and degradation of cyanobacteria significantly modulate the physicochemical properties of the microenvironment of the SWI in terms of pH, oxygen penetration depth (OPD), dissolved organic carbon concentration, and redox potential (ORP), and then uncouple nitrification–denitrification in surface sediment. In addition, when overlying water is covered by densely aggregated algae, a large amount of dissolved organic matter (DOM) continuously releases and migrates during algae decomposition. The degradation and mineralization of organic aggregates could significantly influence the physicochemical properties across the SWI, typically including DO, pH, ORP, electrical conductivity (EC), particle size distribution, and the abundance and activity of microbial communities [12,14–16]. Due to the rapid exhaustion of DO through biodegradation or respiration of the algae, the balance between microbial nitrification and denitrification is largely disrupted in sediments. It leads to consequential anoxic/hypoxic conditions at the SWI, ideal for denitrification, which therefore becomes a hotspot for nitrogen reduction [17,18]. The combination of ubiquitous nitrification and denitrification processes in aquatic ecosystems alleviates the negative impacts of excessive N by transforming reactive N to gaseous forms prior to permanently removing it from lakes [18]. Nitrification provides substrates for denitrification by oxidating ammonium (NH_4^+-N) to nitrite (NO_2^--N) and then nitrate (NO_3^--N) stepwise [19,20], which constitutes an essential process that transforms almost all N fractions and manipulates N accumulation rates. Therefore, it is speculated that the decay of ABs in eutrophic lakes facilitates N cycling processes, resulting in significant variation in the distribution pattern of labile N.

The SWI is the transition zone of aquatic ecosystems, and plays an important role in the storage, transfer, and circulation of biogenic elements and/or contaminants [13]. The complicated biochemical interactions among various fractions along a significantly heterogeneous temporal–spatial scale makes it difficult to quantify the N fractions at the SWI [21,22]. High-resolution techniques with sufficient sensitivity are thus necessary to acquire accurate labile N concentrations during AB decomposition to decipher the distribution, transport, and bioavailability of N fractions. Several methods have been developed to investigate the distribution of and dynamic changes in contaminants at the SWI [23–25]. However, there exist limited investigations of high-resolution descriptions of the migration and transformation of LN fractions. According to Fick's First Law, the diffusive gradients in thin films (DGT) technique overcomes the limitations of ex situ methods by allowing in situ characterization of contaminants. DGT devices selectively accumulate target fractions using diffusive and specific binding gels, which allow the velocity of accumulation to be controlled [24]. Binding gels were primarily prepared from one or two different agents to target specific elements [19]. To optimize the accumulation performance, a mixed binding gel was developed to simultaneously accumulate different labile N fractions to identify the nitrification and denitrification process [26]. Another in situ technique, HR-Peeper, utilizes dialysis to obtain high-resolution information on pore water contamination. It employs a dialysis membrane and recess hole for multi-chambered separation, enabling high-resolution accumulation of target elements from the surrounding pore water at a vertical resolution of 2 mm. Accordingly, the combination of diffusive gradients in DGT and dialysis in HR-Peeper can help obtain high-resolution information on multiple N fractions and dissolved organic matter (DOM) in the vertical profiles of sediment.

This study aimed to investigate the spatial variations in labile NH_4^+-N and NO_3^--N concentrations in the sediment of Taihu, a large shallow eutrophic lake in China. The DGT technique was used to determine labile NH_4^+-N and NO_3^--N, while the HR-Peeper technique was utilized to measure NO_2^--N concentrations. Additionally, the abundance of genes referring to nitrification and denitrification (AOB *amoA* gene, AOA *amoA* gene, and

nosZ gene) in the sediments was characterized using quantitative real-time polymerase chain reaction (qPCR). To understand the influence of anthropogenic activities on DOM variations, an annular flume simulation experiment was adopted to investigate the temporal variations in DOM. The main aims of this study were to (1) obtain high-resolution profiles and visualize the dynamic processes of labile N fractions in the sediments' pore water, (2) characterize DOM variations in the lake under the influence of anthropogenic activities, and (3) clarify the mobilization and transformation processes of N in sediments and the dynamic N exchange at the SWI under eutrophic conditions. Consequently, this investigation proposed to provide insights into the variation in the conversion of N fractions across the SWI in response to the decomposition of anthropogenic inputs in eutrophic freshwater ecosystems.

2. Materials and Methods

2.1. Description of Study Area

Being the third-largest freshwater lake in China, Taihu is a large shallow eutrophic lake located in the southeastern region of the Yangtze River Delta, with a surface area of 2338 km^2, mean depth of 1.9 m, and maximum depth of $\leq$3 m [27,28]. The Taihu Basin is characterized by a complex set of river networks, including 172 rivers, tributaries, and channels draining into the lake. A rapid boom of the economy and population in the basin has significantly increased the load of nutrients discharged into the tributaries of Taihu [29]. The consequent deterioration in lake water quality has been accelerated due to severe and frequent HABs, which have led to serious environmental, economic, and societal problems [30]. Despite a series of operations to control the eutrophication and HABs in Lake Taihu taken by the Chinese government, their magnitude and frequency have not decreased as much as expected from the mitigation efforts [31].

2.2. Sample Collection and In Situ Measurements

Sampling was carried out at 18 sites in June 2021 to represent the status of the Taihu (Figure 1). The labile concentrations of N fraction and DOM in the sediment profiles were measured in situ using the AMP-TH DGT and HR-Peeper devices (EasySensor Ltd., Nanjing, China), respectively. An interface recognition device was designed to accurately identify the SWI for DGT and HR-Peeper deployment as described in the Supplementary Materials. The physical parameters of overlying water were measured using a multisensory probe (YSI-6600, YSI Incorporated, Yellow Springs, OH, USA), including temperature, DO, pH, and ORP. Chlorophyll-a (*Chl-a*) was quantified spectrophotometrically following extraction with 90% acetone for 24 h in the dark at 4 °C [7]. Surface sediments were collected using a Peterson grab sampler (KH0201, VRERA, Changzhou, China) for subsequent determination of microbial abundance. All the samples were delivered to the laboratory immediately on the same day to minimize external interference. Sites 1–10 were located in the AB-dominated regions: the northern and northwestern Zhushan Bay (sites 1–3), Meiliang Bay (sites 4–6), and Gonghu Bay (sites 7–8); the northwestern part of the lake (sites 9–10). Site 11 was located in the center of the lake without the problem of Abs nor the distribution of macrophytes. Sites 12–15 were located in the southeastern bays dominated by macrophytes, where site 15 has been dominated by aquatic vegetation over the years under artificial intervention. Sites 16–18 were located in the southwestern part of Taihu Lake, where macrophytes were completely absent but ABs were occasionally observed. The detailed locations of the sampling sites are presented in Table S1.

2.3. Analysis of Sediment Microbial Abundance

Sediment nitrifier and denitrifier abundances were analyzed using qPCR, for which AOB *amoA*, AOA *amoA*, and *nosZ* marker genes were selected. As reported previously, the AOB *amoA* and AOA *amoA* genes are markers of ammonia-oxidizing bacteria and ammonia-oxidizing archaea, the dominant nitrifiers in Taihu Lake [32,33], and the *nosZ*

gene is a common marker of denitrifiers, encoding nitrous oxide reductase [34]. The qPCR primers and programs are detailed in the Supplementary Materials (Table S2).

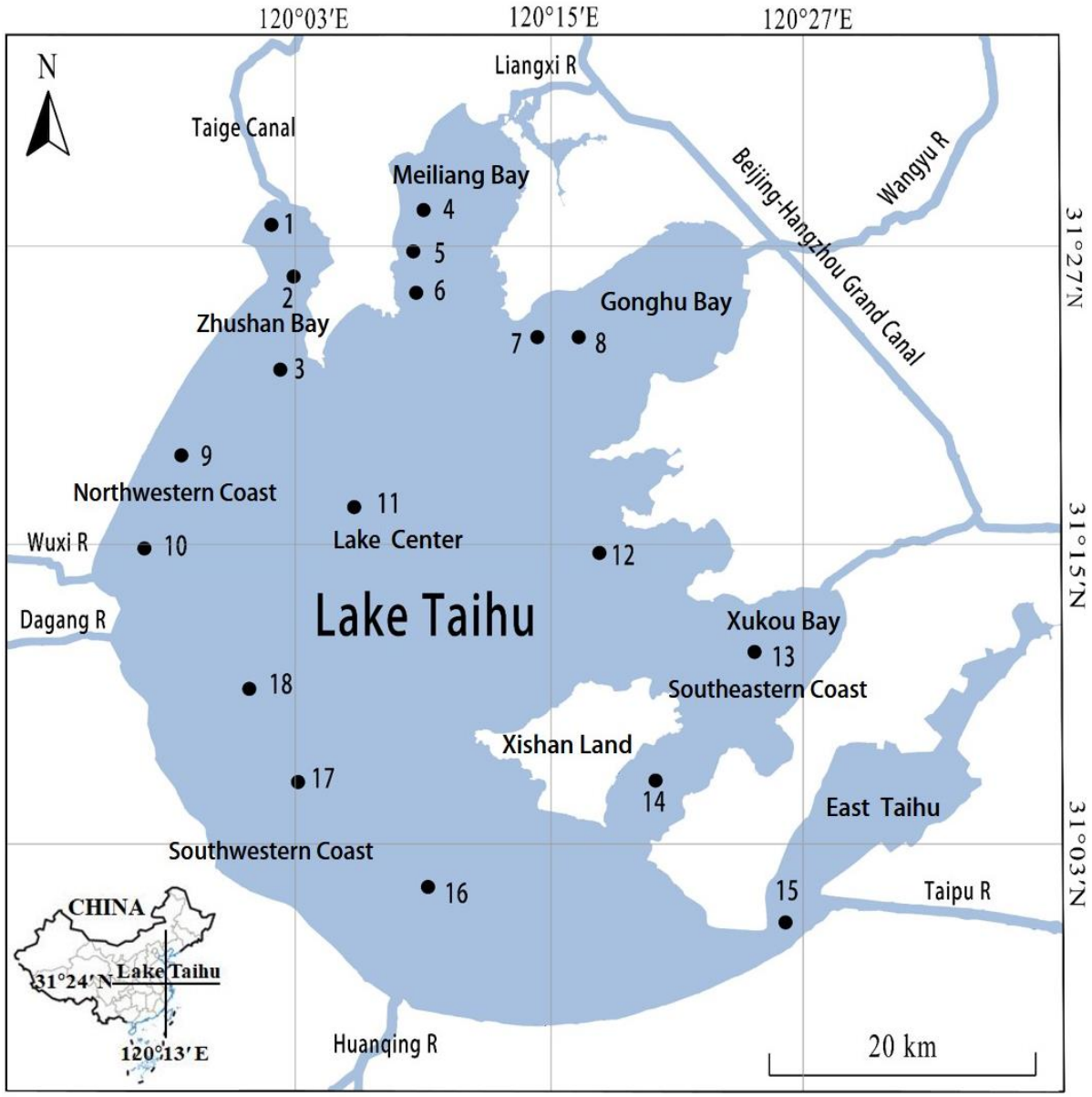

Figure 1. Study area and 18 sampling sites in Taihu Lake, China.

2.4. Flume Simulation Experiment

Sediments were collected from Zhushan Bay (31°24′38″ N, 120°02′12″ E) using a Peterson grab sampler and were immediately delivered to the laboratory for the flume simulation experiment. These sediments were sieved with a 0.6 mm pore size mesh in order to remove large particles and macrofauna, and then added into an annular flume up to 15 cm. This was followed by adding another sediment column to the flume sediments, with the same height as the sediments in the flume. The overlying water collected from Taihu was carefully added by siphoning using 5 silicone tubes with an inner diameter of 5 mm to avoid disturbing the sediments. Overlying water at a height of 30 cm was maintained in the flume and a hood for light proofing was added to the annular flume to prevent massive algal breeding. A blower was set up in the annular flumes with a flow velocity of 0.1 m s^{-1} based on the conditions of the sampling site in Lake Taihu. Additionally, tap water left overnight was added for evaporation replenishment during the experiment. The schematic of the flume is shown in Figure S2. After the sediments were pre-incubated in the flume

for one month, 1000 mL fresh algae from Zhushan Bay was added into the flume to obtain a concentration of *Chl-a* 2.50 mg L^{-1}, similar to that recorded at Zhushan Bay during the algae blooms [35]. The water temperature was also set to 25 °C using an air conditioner. Our previous studies have indicated that the entire decomposition period of ABs varied from 14 days to 42 days, depending on the illumination, wind fluctuation, Abs' biomass, and Abs' vitality. Accordingly, day 0 (K, before adding fresh algae) and days 1, 5, 11, 38, 55, 85, and 108 were chosen as the sampling dates in the simulation experiment. DGT and Peeper were deployed in the sediments, and the sediment column in the flume was taken out to measure the DO and pH value using microelectrodes (OX-100, pH-500, Unisense, Aarhus, Denmark). Subsequently, the sediment column was carefully returned to the flume. The annular flume simulation experiment was used to simulate the decomposition process after the outbreak of ABs in Taihu to help comprehensively understand N transport and transformation under the influence of ABs.

2.5. DGT and HR-Peeper Analysis

Labile NH_4^+-N and NO_3^--N were measured using AMP-TH DGT probes, whereas NO_2^--N and DOM were measured using HR-Peeper. All probes were sealed in containers filled with deoxygenated 0.01 M NaCl solution for DGT tests or deoxygenated water for HR-Peeper tests prior to deployment. The new flat-type DGT device (2 cm × 15 cm) comprises a plastic housing, binding gel, diffusive gel, and filter membrane (Figure S3). After retrieval from sediments, each probe was rinsed with deionized water to carefully remove attached sediment particles. After that, the probes were placed in a container sealed at air temperature before analyses to prevent moisture loss. The AMP-TH binding gels were disassembled from the deployed DGT probes, then sliced vertically and evenly at 2 mm intervals using a cutter with a thickness of 1 mm (Easy Sensor Ltd., Nanjing, China) that was made by stacking ceramic blades. Each slice was eluted using 0.8 mL of 1 M NaCl for 24 h. Nessler's reagent colorimetric method and the ultraviolet spectrophotometric method were used to determine the concentrations of NH_4^+-N and NO_3^--N in the AMP-TH DGT eluents, respectively [36]. Microvolume eluents were measured using the miniaturized spectrophotometry method and the Epoch microplate spectrophotometer (BioTek, Winooski, VT, USA). The calculation of values obtained with DGT is described in the Supplementary Materials.

There are 36 chambers filled with 400 μL deionized water covered by a 0.45 μm cellulose nitrate membrane in the HR-Peeper device and an exposed 4 × 20 cm window providing a 5.0 mm vertical resolution [26,37]. Once the soluble ions and molecules reached equilibrium via diffusion through the dialysis membrane, the solution compositions in the chambers were defined as those of the pore water (Figure S4). After retrieval of the devices, negative internal pressure in the chamber was released by piercing the covering cellulose nitrate membrane with a plastic micropipette tip (200 μL). The collected pore water was then extracted and sequentially injected into a 1.6 mL 96-well microplate. The NO_2^--N concentrations of the pore water were then determined using an Epoch microplate spectrophotometer (BioTek, Winooski, VT, USA). In addition, the pore water in the HR-Peeper chambers was collected to analyze the DOM in the overlying water (3 cm to SWI). A Fluoromax-3 spectrometer (HORIBA Instruments Inc, Sunnyvale, CA, USA) was used to analyze the excitation emission matrix (EEM) fluorescence spectrum of the extracted DOM. The scan speed was set at 12,000 nm min^{-1}, and the scanning ranges of excitation and emission were 200–500 nm and 230–550 nm, with scanning intervals of 5 nm and 0.1 nm. Milli-Q water was used as the blank of EEM, where Raman scatter peaks of the water were eliminated.

2.6. Statistical Analysis

Spatial distributions of the apparent fluxes and concentrations of the DGT N fraction across the SWI were plotted using Origin Pro 2018 64Bit software (Origin Lab Inc., Northampton, MA, USA). SPSS 22 for Windows (SPSS Inc., Chicago, IL, USA) was used for

statistical analysis. The data from DGT-measurements were tested statistically at significant level of $p < 0.05$ using one-way ANOVA (analysis of variance). The relationship between the selected parameters and the DGT-measured concentrations was further analyzed through simple linear regression and the Mantel test. Pearson's correlation analysis was applied to reveal the relationships between the concentrations of dissolved or labile elements and nitrifier/denitrifier abundance. A *t*-test was used to show the significant differences in nitrifier/denitrifier abundance between sites. Significant differences between treatments were accepted at the level of $p < 0.05$. Parallel factor analysis (PARAFAC) was conducted using MATLAB 2019a (Math Works Inc., Natick, MA, USA) software with the DOM Fluor toolbox (http://www.models.life.ku.dk/, accessed on 30 June 2022), and the outliers were removed through Rayleigh and Raman scattering correction.

3. Results and Discussion

3.1. Physicochemical Properties of the Water Layer above the Sediment

The physicochemical properties of the overlying water were analyzed at each sampling site as presented in Table 1. The dissolved oxygen (DO) concentration ranged from 5.35 to 9.58 mg L^{-1} across all sampling sites. It was observed that the northern sampling sites of Taihu generally had lower DO concentrations compared to the southern sites. This difference can be attributed to higher algal biomass in the northern sites, which consumes oxygen through respiration. The oxidation–reduction potential (ORP) values ranged from 244.8 to 299.1 mV, indicating an oxidized condition in the water layer at all sampling sites. The pH values of the water layer varied from 7.30 to 8.34, indicating weak alkalinity. The chlorophyll-a (Chl-a) concentration varied greatly among the sampling sites, ranging from 12.26 to 249.33 μgL^{-1}. This indicates that all sampling sites were in a eutrophic or hypereutrophic state according to the Chl-a thresholds defined by Zhou et al. [9]. The ammonium nitrogen (NH_4^+-N) concentrations ranged from 1.23 to 12.37 mg L^{-1}, while the nitrate nitrogen (NO_3^--N) concentrations ranged from 2.39 to 7.91 mg L^{-1}. Additionally, the nitrite nitrogen (NO_2^--N) concentrations ranged from 0.03 to 0.20 mg L^{-1}.

Table 1. Physicochemical properties of overlying water at 18 sampling sites in Taihu Lake, China.

Sample Sites	DO (mg L^{-1})	ORP (mV)	pH	Chl-a (μg L^{-1})	NH_4^+-N (mg L^{-1})	NO_3^--N (mg L^{-1})	NO_2^--N (mg L^{-1})
1	5.73	273.3	7.60	15.17	5.98	7.91	0.03
2	5.67	261.7	7.68	137.38	12.37	2.69	0.05
3	6.75	249.7	8.18	80.97	3.65	7.07	0.05
4	6.77	244.8	8.01	105.12	2.66	3.75	0.04
5	6.65	247.0	8.09	15.58	1.80	4.12	0.20
6	6.65	249.4	8.13	13.83	3.60	4.78	0.04
7	8.83	263.0	8.34	58.54	5.11	6.73	0.04
8	7.23	269.0	8.26	47.13	3.25	4.82	0.08
9	5.35	269.6	7.61	12.26	8.89	3.68	0.17
10	9.58	267.4	8.11	112.26	12.15	2.39	0.06
11	8.65	284.2	7.39	89.89	5.74	7.00	0.07
12	8.66	251.7	7.54	23.25	1.23	5.11	0.05
13	8.72	276.6	7.64	13.93	10.42	6.25	0.05
14	9.22	282.6	7.74	13.57	11.44	4.84	0.07
15	7.43	286.8	7.30	34.05	8.73	5.52	0.08
16	9.04	299.1	7.47	47.79	2.78	7.32	0.07
17	9.09	290.6	7.65	44.83	8.27	7.41	0.12
18	9.02	289.8	7.72	249.33	8.13	7.08	0.15

3.2. Profiles of Nitrogen Fractions in the Sediments

The distributions of labile NH_4^+-N in the sediment were examined using DGT measurements, and the average concentrations at each depth are depicted in Figure 2. The profiles of labile NH_4^+-N showed different variation patterns among the sites, indicating

high heterogeneity. Two distinct patterns were observed in the one-dimensional profiles. In the first pattern, the concentration of labile NH_4^+-N increased sharply towards the sediment surface (depth of 20~−20 mm, with negative values indicating depth below the SWI), then decreased and became stable towards the bottom of the sediment. This pattern was observed in 12 sites (sites 1, 2, 5, 9–11, and 13–18). Notably, sites 14, 15, and 16, located in the southern part of Taihu and dominated by macrophytes, exhibited wider peaks. In the second pattern, the labile NH_4^+-N concentration remained relatively stable in the water layer above the sediment and then increased sharply towards the sediment surface (depth range of 10~−10 mm), after which it exhibited little variation with depth. The concentration of labile NH_4^+-N in the water layer was significantly lower than that in the sediment. This pattern was observed in six sites (sites 3, 4, 6–8, and 12) located in the northern part of Taihu, which were frequently dominated by algal blooms.

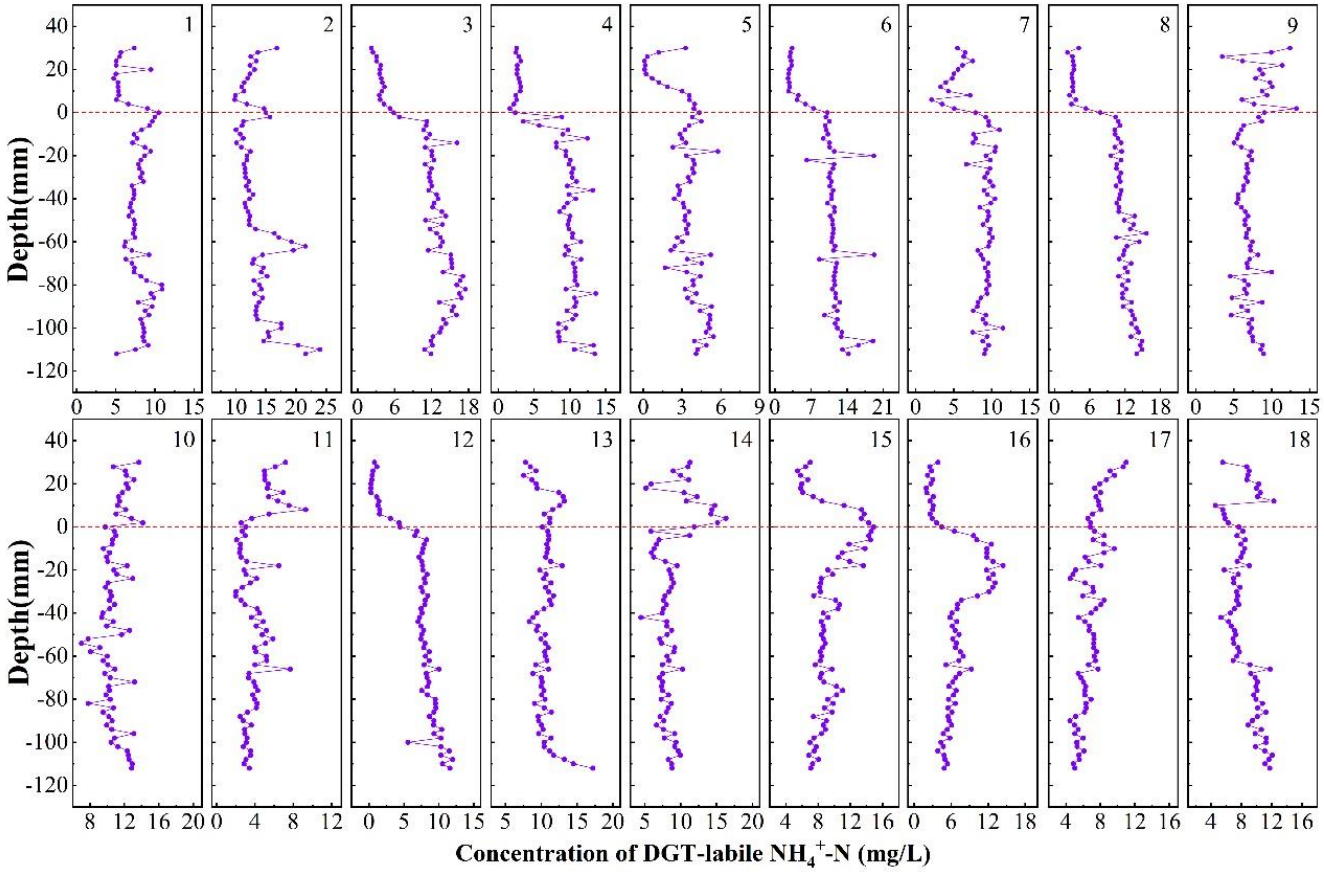

Figure 2. Vertical distribution of labile NH_4^+-N in sediment profiles of 18 sampling sites in Taihu Lake, China. The dotted lines at the depth of zero show the position of the sediment–water interface (SWI).

The distribution of labile NO_3^--N concentrations at sites 1–12, 17, and 18 showed an obvious diffusion gradient in the SWI (Figure 3). The labile NO_3^--N profiles showed an opposite trend to the second pattern of labile NH_4^+-N distribution, which remained high in the overlying water and sharply decreased downward in the range of 10~−10 mm, after which the concentration distributions exhibited little variation with depth. In contrast, the labile NO_3^--N concentrations at sites 14–16 increased downward in the range of 10~−10 mm. These results provide evidence of diffusion of major nitrogen fractions between the overlying water and sediment in the SWI. However, labile NO_3^--N concentrations at site 13 did not change significantly in comparison.

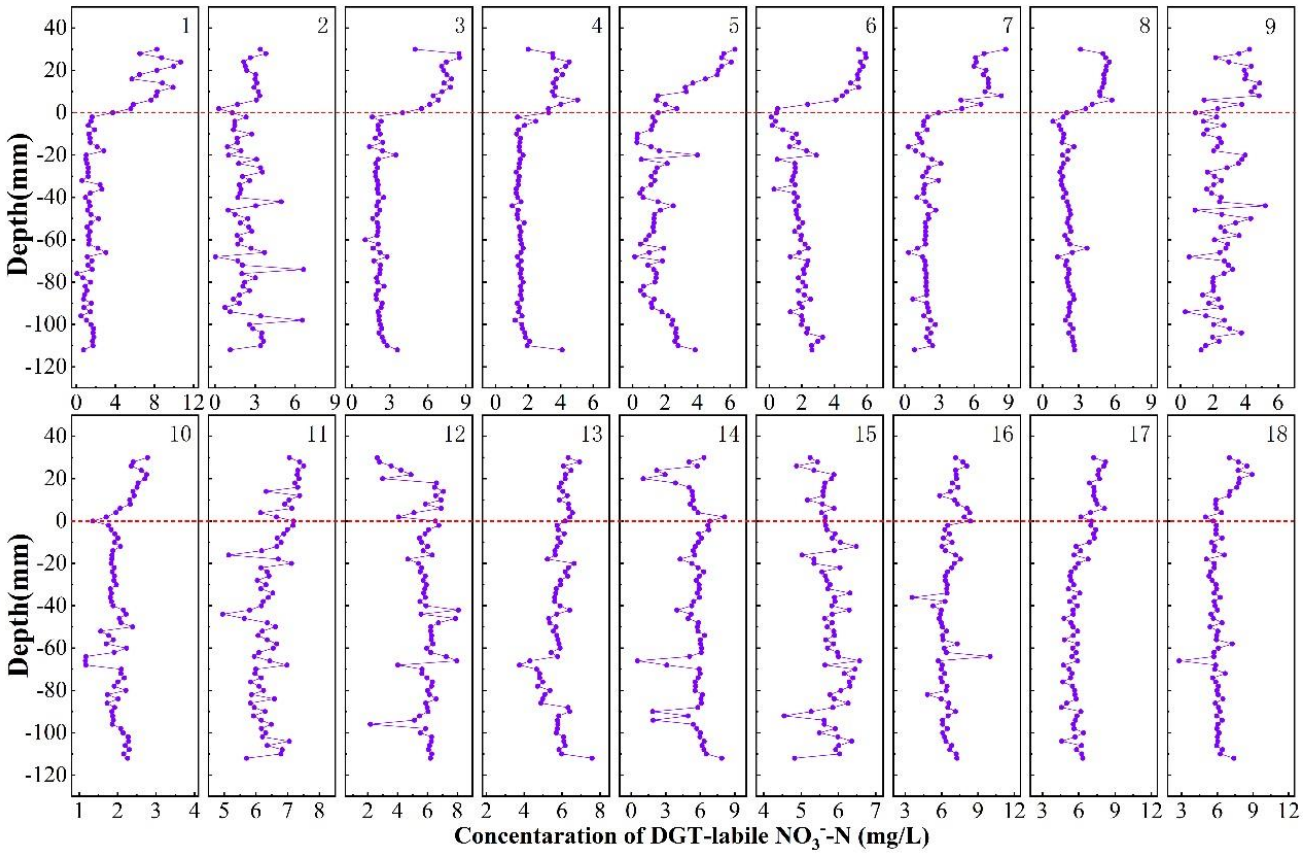

Figure 3. Vertical distribution of labile NO_3^--N in sediment profiles of 18 sampling sites in Taihu Lake, China. The dotted lines at the depth of zero show the position of the sediment–water interface (SWI).

The distribution of NO_2^--N in the sediment profiles was determined using HR-Peeper (Figure S5). The NO_2^--N profiles' distribution was similar to that of NO_3^--N at most sites, with the NO_2^--N concentration decreasing with depth or remaining relatively constant in the range of 20~−20 mm. However, sites 16 and 17 showed an increase with depth in the range of 20~−20 mm, and the NO_2^--N concentrations in the profiles were low, owing to the fact that NO_2^--N was easily oxidized to NO_3^--N, which was an intermediate product of the nitrification process.

Fluctuations in the DGT-labile N fraction curves of the sediment profiles could be attributed to bioturbation by organisms such as *Chironomus larvae* and *Corbicula fluminea* [24]. Moreover, the sediments were highly heterogeneous, and the partition of the horizontal variability in labile N profiles could demonstrate a corresponding change in N lability originating from the sedimentation history and/or mechanistic processes [38]. Notably, concentration gradients were observed in the labile N fraction in the SWI at most sites in this study. This phenomenon has also been reported for phosphorus, sulfide, and metal ions in lake sediment profiles [12,38,39]. Few studies have been carried out on the distribution of labile N fractions in lake sediments, and significant differences in the distribution patterns of labile N fractions at the different sites observed in this study have rarely been reported. It is proved that high-resolution measurements have facilitated the deciphering of this phenomenon.

3.3. Apparent Diffusion Flux of N across the SWI

Diffusion fluxes of labile NH_4^+-N, NO_3^--N, and NO_2^--N across the SWI of all lake sediments were calculated based on Fick's First Law (Figure 4), where positive or negative values indicate an upward or downward diffusion flux, respectively. The apparent diffusion fluxes of labile NH_4^+-N at the SWI ranged from −72.72 to 109.71 mg $m^{-2}d^{-1}$. Except for sites 9, 11, 17, and 18, which showed negative values, the other sites showed positive

values. The apparent diffusion fluxes of labile NO_3^--N and NO_2^--N at the SWI ranged from −40.13 to 34.56 mg $m^{-2}d^{-1}$ and −2.05 to 0.78 mg $m^{-2}d^{-1}$, respectively. Labile NO_3^--N fluxes showed positive values at sites 13, 14, and 16, while the other sites showed negative values. Similarly, labile NO_2^--N fluxes showed positive values at sites 3, 16, and 17, whereas the other sites showed negative values.

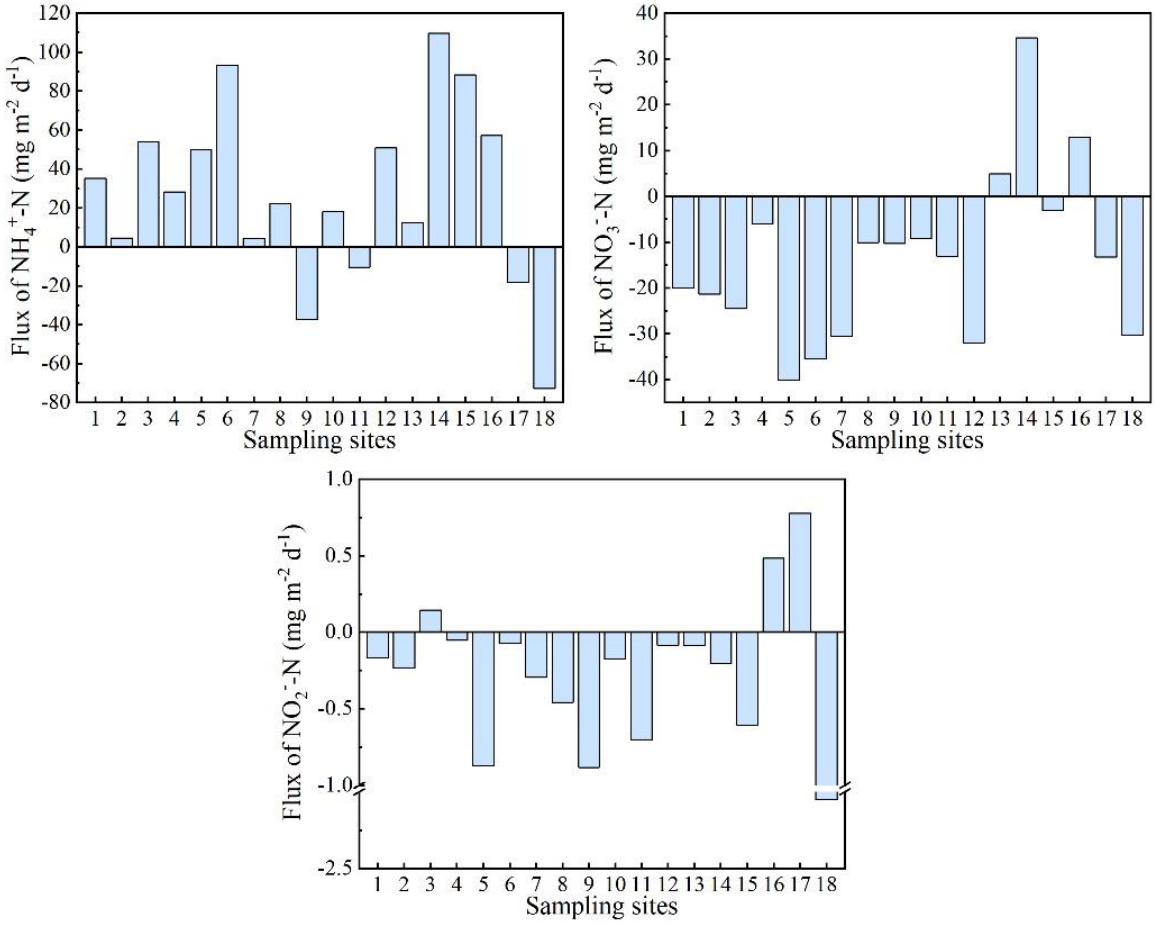

Figure 4. The apparent diffusion flux of the labile NH_4^+-N, NO_3^--N, and NO_2^--N across the sediment–water interface (SWI) of 18 sampling sites in Taihu Lake, China. Positive (negative) values indicate an upward (downward) diffusion flux.

3.4. Absolute Abundance of Functional Genes in Sediment

Significant variation was observed in the abundance of nitrification and denitrification genes between sampling sites. The abundance of the AOB *amoA*, AOA *amoA*, and *nosZ* genes at the sampling sites varied from 5.81×10^6 to 6.31×10^8 copies/g, from 2.96×10^5 to 4.16×10^8 copies/g, and from 5.30×10^7 to 1.07×10^9 copies/g, respectively (Figure 5). The abundance of nitrification and denitrification genes was significantly higher at sites 1, 5, 6, and 9, all of which were located in the northern region of Taihu and were frequently dominated by Abs. Additionally, Pearson correlation analysis indicated that the abundance of the AOB *amoA*, AOA *amoA*, and *nosZ* genes had significant positive relationships ($p < 0.01$). Although no significant correlation was observed between gene abundance and NH_4^+-N, NO_3^--N, or NO_2^--N concentrations ($p < 0.05$), previous studies observed that in various environments the nitrification and denitrification rates could be related to the abundance of relative gene copies [40,41]. Therefore, high rates of nitrification and denitrification were likely present at sites 1, 5, 6, and 9 in Taihu.

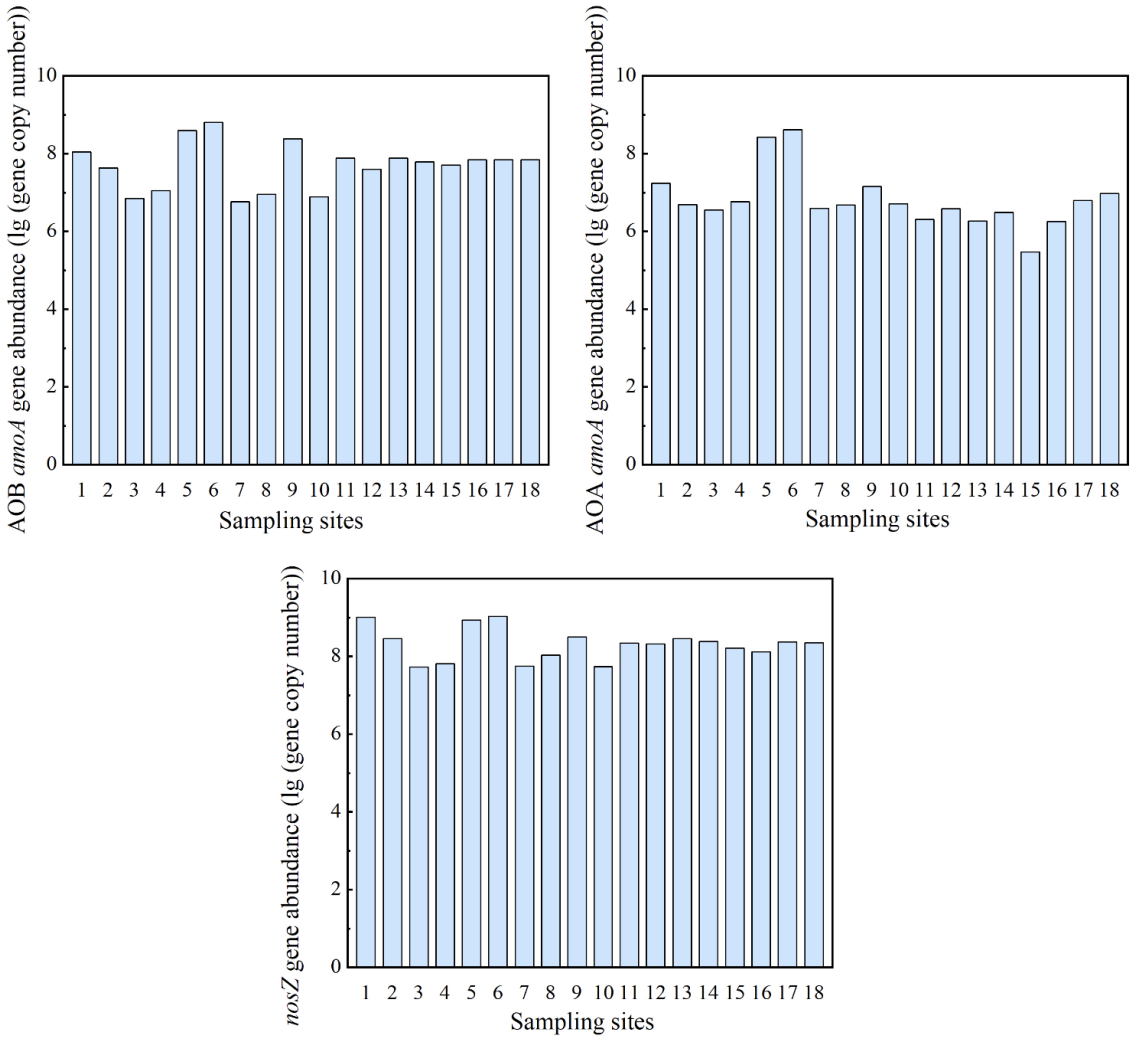

Figure 5. The abundance of AOB *amoA*, AOA *amoA*, and *nosZ* genes in 18 sampling sites' sediments from Taihu Lake, China.

The distribution characteristics of N fractions and microorganisms at different sampling sites may differ significantly due to the decay and decomposition of algae. To further investigate this, a flume simulation experiment was conducted after field surveys to comprehensively understand N transport and transformation under the influence of ABs.

3.5. The Impact of Algal Decomposition on Dissolved Oxygen and pH

Algal decomposition had a significant influence on DO concentrations and the penetration depth across the SWI. Before the outbreak of ABs, DO concentrations ranged from 215.17 to 227.70 μmol L^{-1}, and the penetration depth was approximately 10 mm (Figure S6). However, after the addition of algae on day 1, DO depletion occurred dramatically, leading to anoxia/hypoxia at the SWI. Small molecular dissolved organic matter (DOM) fills the sediment pores during algal decomposition, on account of the oxygen consumption. Additionally, the mineralization of organic matter generally results in a depletion of DO [42]. The overlying water gradually re-oxygenated with the collapse and complete decomposition of algal colonies. It was not until day 55 that the DO level of the overlying water and OPD in sediment recovered to pre-algal addition levels. Thus, changes in the DO concentrations and oxygen penetration depth indicate that algal decomposition has a significant impact on DO consumption in the sediments of algae-dominated zones, which often leads to a subsequent decline in water quality, and fish death and biodiversity loss in lake ecosystems.

Furthermore, algal decomposition also contributed to significant variations in vertical pH across the SWI due to the release of carbon dioxide and organic acids [35]. Both the overlying water and sediments exhibited weakly alkaline pH, with the values of the overlying water being slightly higher than those of the sediments (Figure S7). The magnitude of pH fluctuations within the sediment decreased below depths of approximately −20 to −30 mm, which were deeper than that of OPD. The maximum pH value in the sediment profiles appeared at the SWI. After the addition of algae on day 1, the pH value at the SWI decreased significantly from 9.11 before the addition of algae to 8.73. However, the pH values at the SWI recovered to their initial values by day 55. In anoxic sediments, microbial processes such as the reduction of iron (III), manganese (IV), and sulfate could induce an increase in pH, which might counteract the effect of carbon dioxide and organic acids [43]. Therefore, the pH value only decreased significantly at the SWI, where the DO concentration was the highest.

3.6. Impact of Algal Decomposition on DOM Variation

Algae is one of the most important DOM sources. The variation in EEM fluorescence with time during algal decay is shown in Figure S8. PARAFAC was applied to further characterize and identify individual fluorescent groups in the EEM fluorescence. Four unique fluorescent components were identified (Figure S9). Component 1 (C1) was assigned to terrestrial humic-like components, which are widespread in freshwater ecosystems and are associated with high-weight aromatic molecules [44,45]. Component 2 (C2) was tentatively identified as a fulvic acid and allochthonous humic-like substance [46,47]. Component 3 (C3) was determined to be a humic-like component that occurs in fresh waters and oceans [48]. C3 was correlated with biological activity, which could include potential microbial reprocessing and/or phytoplankton degradation [49–52]. Component 4 (C4) was mainly composed of tyrosine and protein-like substances, which primarily originated from the degradation of microalgae and substantially humic-like components during transformation [47,53]. Thus, the main fluorescent components of DOM in the overlying water during algal decay were humic-like components, which could subsequently form organic colloids and organic–inorganic ligands, stimulating the release of internal phosphorus and nutrients for continuous ABs in the eutrophic lake.

Furthermore, the maximum fluorescence intensity (F_{max}) of each component demonstrates the concentration of fluorescent DOMs (Figure S10). The F_{max} of C1, C2, and C4 increased sharply after the algal outbreak and decreased with algae decomposition, remaining at a low level after day 55. However, the fluorescence intensity of C3 did not decrease over time after reaching F_{max}. The results indicated that C1, C2, and C4 were readily available components, while C3 was recalcitrant for biodegradation. The F_{max} of C1 correlated positively and significantly with the F_{max} of C2 ($r^2 = 0.803$, $p < 0.05$), and the F_{max} of C2 correlated positively and significantly with the F_{max} of C4 ($r^2 = 0.905$, $p < 0.01$). This indicates reciprocal transformations between C1 and C2, and C2 and C4, closely associated with the algal biomass, respectively [54].

3.7. Impact of Algal Decomposition on Nitrification and Denitrification

The distribution pattern of NH_4^+-N in the sediment changed with the algae decay (Figure S11). On days 1, 5, and 11, a prominent obvious concentration peak was observed at the SWI, which belonged to the first pattern of NH_4^+-N distribution. However, from day 38, the concentration peak disappeared, steep concentration gradients were observed at the SWI, and the vertical distribution of NH_4^+-N (the second pattern of NH_4^+-N distribution) became visible. Control K, which was not affected by algae, also showed the second pattern, indicating that algae decomposition significantly changed the distribution pattern of NH_4^+-N in the sediment. Accordingly, the peak of NH_4^+-N concentrations in the SWI might be attributed to algal decomposition. Furthermore, on day 1 of algae addition to the flumes, the profiles of the NH_4^--N and NO_3^--N concentrations were lower than that of the control owing to the prompted release of N from the sediment into the overlying water where

algal growth absorbs labile N (Figure S12). Later, algae decomposition increased NO_3^--N and NO_2^--N concentrations in the overlying water to levels higher significantly than those in the sediment (Figures S12 and S13). It is suggested that this triggered the nitrifying community, which helped to restart the coupled loop of nitrification–denitrification [55]. The difference in concentration gradients between the sediment and overlying water decreased with the progressive decomposition of the algae.

Additionally, the algal bloom completely altered the function of the sediment sources and sinks (Figure 6). Before the addition of algae, the apparent diffusion flux of NH_4^+-N was negative and that of NO_3^--N and NO_2^--N was positive in the sediment, indicating that the sediment played the role of a sink for NH_4^+-N, and source of NO_3^--N and NO_2^--N. However, after the addition of algae, a completely reverse diffusion flux was observed (except on days 55 and 85, when the flux of NO_2^--N was positive), and the sediments became a source of NH_4^+-N and a sink for NO_3^--N and NO_2^--N. Previous studies have shown that the time of flux reversal is related to the density of algae, with an earlier reversal attributed to a higher algal density [13]. The results of the laboratory flume simulation experiment were consistent with the diffusive flux results from the field investigation in Taihu, indicating that the change in the direction of the diffusive flux was correlated with the algal decay. A positive diffusive flux of NH_4^+-N was observed during algal decay due to a large amount of algal sinking in the SWI and a substantial release of NH_4^+-N into the overlying water from the decomposed algal cells. Thereafter, NH_4^+-N was oxidized to NO_2^--N and NO_3^--N through nitrification in the aerobic layer [17], because of which an increase in the NO_2^--N and NO_3^--N concentration in the overlying water occurred. The diffusion of NO_2^--N and NO_3^--N from the overlying water into the sediment along the concentration gradient was finally removed through denitrification under anaerobic conditions [23]. Thus, algal decay contributes to the removal of N from eutrophic lakes.

A previous investigation has reported that the duration of algae deposition after algae addition varied from 14 to 42 days, depending on the actual physicochemical properties [56]. Aggregates produced by the decaying algae were deposited to the SWI to form a benthic bioclastic mat, which amplified the scope of the anaerobic area in the SWI [39,57], leading to a predominance of denitrification (Figure 7). However, the water column is not continuously anoxic in shallow lakes because of wind and wave disturbances, which could alleviate oxygen penetration into sediments and increase the amount of available oxygen for nitrification [34]. Furthermore, most nitrifying bacteria tend to inhabit spaces with lower or limited oxygen, such as the oxic–anoxic interface. Thus, the NH_4^+-N released by algal decay was transformed into NO_3^--N and NO_2^--N through nitrification, resulting in an accumulation of NO_3^--N and NO_2^--N at the SWI. The sediments became sinks rather than sources of NO_3^--N and NO_2^--N, which provided sufficient substrate for denitrification. In addition, the rapid degradation of algae dramatically produces large amounts of DOM, thus providing an additional carbon source for denitrifiers and triggering the growth of microorganisms. As a result, denitrification was accelerated in deeper anoxic sediments, which accelerated nitrogen removal from the water column and greatly improved denitrification efficiency. With further complete decomposition of the AB residues, the quality of the water column gradually recovered and the depth of DO penetration increased, leading to nitrification becoming the main reaction. Consequently, deep microporous aeration is recommended to increase DO availability in the SWI in eutrophic lakes.

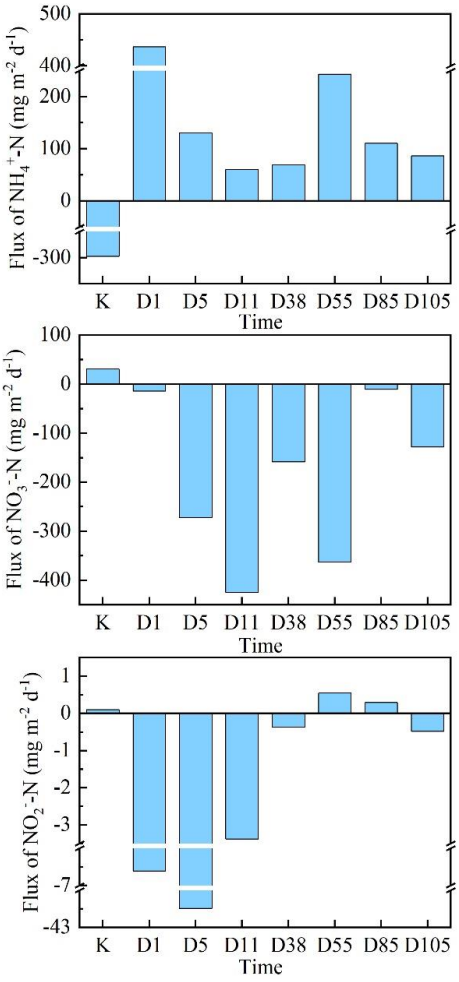

Figure 6. The apparent diffusion flux of the labile NH_4^+-N, NO_3^--N, and NO_2^--N across the sediment–water interface (SWI) in flume simulation experiment. Positive (negative) values indicate an upward (downward) diffusion flux.

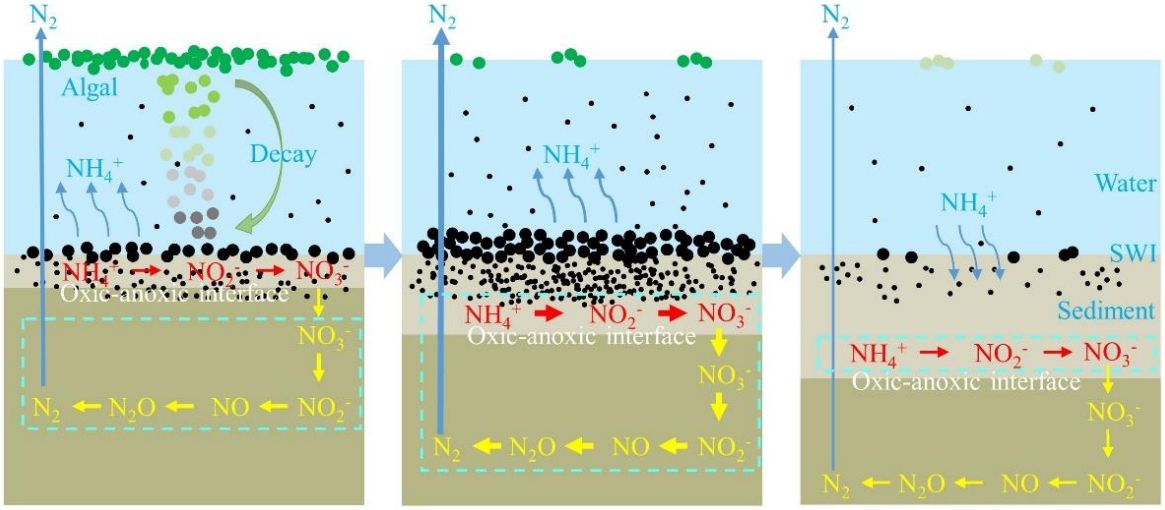

Figure 7. Conceptual diagram of labile N cycling at the sediment–water interface (SWI) influenced by algal blooms (ABs) through the process of algal decomposition in eutrophic freshwater lake ecosystem.

4. Conclusions

High-resolution in situ techniques were applied in field investigation and flume simulation experiments to decipher the transformation and transport of labile N under the

presence of ABs in lakes. This study indicated that the decomposition of ABs could induce an increase in DOM concentration and a decrease in DO penetration depth and pH in the SWI, which resulted in the concentrations of labile N increasing at the sediment–water interface (SWI) with altered diffusion patterns in the sediments. According to the present study, ABs stimulate the release of NH_4^+-N, which is subsequently transformed into NO_3^--N and NO_2^--N through nitrification. This conversion leads to a significant increase in the concentrations of NO_3^--N and NO_2^--N at the sediment–water interface. The decomposition of algae also causes an increase in the concentration of dissolved organic matter, a decrease in dissolved oxygen penetration depth, and a reduction in pH near the SWI. These changes promote denitrification processes in the sediments. Additionally, the decomposition process impacts the distribution patterns of nitrogen and the convertible role of sediments as either a "source" or a "sink" of nitrogen. This investigation provides evidence regarding the migration and transformation of nitrogen fractions and offers insights into the dynamic processes occurring at the SWI in eutrophic lakes. However, the dynamics of N were shown to be seasonally limited, and our field investigation was conducted only once during the AB outbreak in summer. Consequently, further investigations in different seasons are necessary for a better understanding of N transformation and transport in eutrophic lakes.

Supplementary Materials: The following supporting information can be downloaded at: https://www.mdpi.com/article/10.3390/w16020341/s1, Figure S1: The schematic of DGT deployment device. (A) In-situ deployment of DGT and HR-Peeper probes in Lake Taihu; (B) Plastic discs for identifying the sediment-water interface; Figure S2: Schematic of the annular flume. (A) shows the plan form; (B) shows profiles of annular flume; (C) is the picture of annular flume. To avoid the excessive crosswise disturbance of the wind, the sediment cores were deployed in the annular flume which on the opposite side of the blower equipment; Figure S3: Structure of the traditional flat-type diffusive gradients in thin-film (DGT) device (a) and the new flat-type DGT device (b), the DGT device comprises plastic housing, binding gel, diffusive gel, and filter membrane; Figure S4: The structure of the HR-Peeper. (a) the HR-Peeper was assembled by base plate, plastic window, outer frame and inter frame, in the assembly of the HR-Peeper, the chambers were filled with deionized water and covered with a cellulose nitrate membrane (i.e., dialysis membrane; Whatman, 0.45 μm pore size), all the components were bound together using plastic fastener. (b) the lateral view and elevation view of HR-Peeper; Figure S5: Vertical distribution of labile NO_2^--N in sediment profiles of 18 sampling sites in Lake Taihu, China. The dotted lines at the depth of zero show the position of the SWI; Figure S6: Dissolved oxygen concentration variation of sediment profile during ABs decay. The dotted lines at the depth of zero show the position of the SWI; Figure S7: The pH variation of sediment profile during ABs decay. (The computer connected to the microelectrode system failed on day 11 and the data could not be re-determine, resulting in a straight line in the profile). The dotted lines at the depth of zero show the position of the SWI; Figure S8: The variation of excitation emission matrix fluorescence of the concentration of DOM in the overlying water during ABs decay; Figure S9: Four unique fluorescent components of DOM in the overlying water during ABs decay; Figure S10: The maximum fluorescence intensity (Fmax) of each component during ABs decay; Figure S11: Vertical distribution of labile NH_4^+-N in sediment profiles during ABs decay. The dotted lines at the depth of zero show the position of the SWI; Figure S12: Vertical distribution of labile NO_3^--N in sediment profiles during ABs decay. The dotted lines at the depth of zero show the position of the SWI; Figure S13: Vertical distribution of labile NO_2^--N in sediment profiles during ABs decay. The dotted lines at the depth of zero show the position of the SWI; Table S1: Geographic information of the 18 sampling sites in Lake Taihu, China; Table S2: The qPCR primers and programs. References [58–62] are cited in the Supplementary Materials.

Author Contributions: Conceptualization, Y.Y., Y.C. and R.H.; methodology, Y.Y., C.S. and R.H.; validation, Y.C., D.C. and X.H.; formal analysis, Y.F., C.S. and Y.Y.; investigation, Y.C., D.C. and X.H.; writing—original draft preparation, Y.C., H.M. and Y.Y.; writing—review and editing, R.H., H.M., Y.F. and C.S.; visualization, Y.C. and Y.F.; supervision, R.H.; project administration, R.H.; funding acquisition, R.H. All authors have read and agreed to the published version of the manuscript.

Funding: This research was funded by the National Natural Science Foundation of China, grant numbers 41773081 and 42007333; Jiangsu Agricultural Science and Technology Innovation Fund, China (grant number CX (21)3165); the Natural Science Research Project of Higher Education in Jiangsu Province, grant number 20KJB610006; and the Startup Research Foundation for High-level Professionals of Nanjing Normal University, grant number 184080H202B228.

Data Availability Statement: All available data are contained within the article.

Conflicts of Interest: The authors declare that they have no known competing financial interest or personal relationships that could have appeared to influence the work reported in this paper.

References

1. Ho, J.C.; Michalak, A.M.; Pahlevan, N. Widespread global increase in intense lake phytoplankton blooms since the 1980s. *Nature* **2019**, *574*, 667–670. [CrossRef]
2. Hou, X.; Feng, L.; Dai, Y.; Hu, C.; Gibson, L.; Tang, J.; Lee, Z.; Wang, Y.; Cai, X.; Liu, J.; et al. Global mapping reveals increase in lacustrine algal blooms over the past decade. *Nat. Geosci.* **2022**, *15*, 130–134. [CrossRef]
3. Huisman, J.; Codd, G.A.; Paerl, H.W.; Ibelings, B.W.; Verspagen, J.M.H.; Visser, P.M. Cyanobacterial blooms. *Nat. Rev. Microbiol.* **2018**, *16*, 471–483. [CrossRef]
4. Mooney, R.J.; Stanley, E.H.; Rosenthal, W.C.; Esselman, P.C.; Kendall, A.D.; McIntyre, P.B. Outsized nutrient contributions from small tributaries to a Great Lake. *Proc. Natl. Acad. Sci. USA* **2020**, *117*, 28175–28182. [CrossRef]
5. O'Neil, J.M.; Davis, T.W.; Burford, M.A.; Gobler, C.J. The rise of harmful cyanobacteria blooms: The potential roles of eutrophication and climate change. *Harmful Algae* **2012**, *14*, 313–334. [CrossRef]
6. Chen, M.; Ding, S.; Wu, Y.; Fan, X.; Jin, Z.; Tsang, D.C.W.; Wang, Y.; Zhang, C. Phosphorus mobilization in lake sediments: Experimental evidence of strong control by iron and negligible influences of manganese redox reactions. *Environ. Pollut.* **2019**, *246*, 472–481. [CrossRef]
7. Xu, H.; Paerl, H.W.; Zhu, G.; Qin, B.; Hall, N.S.; Zhu, M. Long-term nutrient trends and harmful cyanobacterial bloom potential in hypertrophic Lake Taihu, China. *Hydrobiologia* **2016**, *787*, 229–242. [CrossRef]
8. Yin, G.; Hou, L.; Liu, M.; Liu, Z.; Gardner, W.S. A novel membrane inlet mass spectrometer method to measure $^{15}NH_4^+$ for isotope-enrichment experiments in aquatic ecosystems. *Environ. Sci. Technol.* **2014**, *48*, 9555–9562. [CrossRef] [PubMed]
9. Zhou, J.; Han, X.; Brookes, J.D.; Qin, B. High probability of nitrogen and phosphorus co-limitation occurring in eutrophic lakes. *Environ. Pollut.* **2022**, *292*, 118276. [CrossRef] [PubMed]
10. Li, X.F.; Hou, L.J.; Liu, M.; Zheng, Y.L.; Yin, G.Y.; Lin, X.B.; Cheng, L.; Li, Y.; Hu, X.T. Evidence of Nitrogen Loss from Anaerobic Ammonium Oxidation Coupled with Ferric Iron Reduction in an Intertidal Wetland. *Environ. Sci. Technol.* **2015**, *49*, 11560–11568. [CrossRef] [PubMed]
11. Zhu, J.; He, Y.; Zhu, Y.S.; Huang, M.S.; Zhang, Y.P. Biogeochemical sulfur cycling coupling with dissimilatory nitrate reduction processes in freshwater sediments. *Environ. Rev.* **2018**, *26*, 121–132. [CrossRef]
12. Yao, Y.; Li, D.; Chen, Y.; Liu, H.; Wang, G.; Han, R. High-resolution distribution of internal phosphorus release by the influence of harmful algal blooms (HABs) in Lake Taihu. *Environ. Res.* **2021**, *201*, 111525. [CrossRef]
13. Sima, W.; Hu, M.; He, Q.; Qiu, Y.; Lv, Y.; Dai, L.; Shao, Q.; Zhou, T.; Li, H.; Zhou, M.; et al. Regulation of nitrogen dynamics at the sediment-water interface during HAB degradation and subsequent reoccurrence. *RSC Adv.* **2020**, *10*, 13480–13488. [CrossRef]
14. Jiang, X.; Gao, G.; Zhang, L.; Tang, X.; Shao, K.; Hu, Y. Denitrification and dissimilatory nitrate reduction to ammonium in freshwater lakes of the Eastern Plain, China: Influences of organic carbon and algal bloom. *Sci. Total Environ.* **2020**, *710*, 136303. [CrossRef]
15. Sharp, J.H. Estuarine oxygen dynamics: What can we learn about hypoxia from long-time records in the Delaware Estuary? *Limnol. Oceanogr.* **2010**, *55*, 535–548.
16. Shen, Q.S.; Liu, C.; Zhou, Q.L.; Shang, J.G.; Zhang, L.; Fan, C.X. Effects of physical and chemical characteristics of surface sediments in the formation of shallow lake algae-induced black bloom. *J. Environ. Sci.* **2013**, *25*, 2353–2360. [CrossRef] [PubMed]
17. Shen, Y.S.; Huang, Y.Y.; Hu, J.; Li, P.P.; Zhang, C.; Li, L.; Xu, P.; Zhang, J.Y.; Chen, X.C. The nitrogen reduction in eutrophic water column driven by Microcystis blooms. *J. Hazard. Mater.* **2020**, *385*, 9. [CrossRef]
18. Shi, W.; Zhu, L.; Van Dam, B.; Smyth, A.R.; Deng, J.; Zhou, J.; Pan, G.; Yi, Q.; Yu, J.; Qin, B. Wind induced algal migration manipulates sediment denitrification N-loss patterns in shallow Taihu Lake, China. *Water Res.* **2021**, *209*, 117887. [CrossRef]
19. Kessler, A.J.; Glud, R.N.; Cardenas, M.B.; Cook, P.L.M. Transport Zonation Limits Coupled Nitrification-Denitrification in Permeable Sediments. *Environ. Sci. Technol.* **2013**, *47*, 13404–13411. [CrossRef]
20. Xia, X.H.; Jia, Z.M.; Liu, T.; Zhang, S.B.; Zhang, L.W. Coupled Nitrification-Denitrification Caused by Suspended Sediment (SPS) in Rivers: Importance of SPS Size and Composition. *Environ. Sci. Technol.* **2017**, *51*, 212–221. [CrossRef]
21. Sun, Q.; Ding, S.M.; Wang, Y.; Xu, L.; Wang, D.; Chen, J.; Zhang, C.S. In-situ characterization and assessment of arsenic mobility in lake sediments. *Environ. Pollut.* **2016**, *214*, 314–323. [CrossRef]
22. Wu, Z.H.; Jiang, X.; Wang, S.H.; Zhao, L.; Jiao, L.X.; Chen, J.Y.; Cai, Q.; Wang, K.; Yao, C. Mobilization and geochemistry of nutrients in sediment evaluated by diffusive gradients in thin films: Significance for lake management. *J. Environ. Manag.* **2021**, *292*, 112770.

23. Chen, X.F.; Jiang, H.Y.; Sun, X.; Zhu, Y.; Yang, L.Y. Nitrification and denitrification by algae-attached and free-living microorganisms during a cyanobacterial bloom in Lake Taihu, a shallow Eutrophic Lake in China. *Biogeochemistry* **2016**, *131*, 135–146. [CrossRef]
24. Wang, C.; Yao, Y.; Wang, P.; Hou, J.; Qian, J.; Yuan, Y.; Fan, X. In situ high-resolution evaluation of labile arsenic and mercury in sediment of a large shallow lake. *Sci. Total Environ.* **2016**, *541*, 83–91. [CrossRef]
25. Wu, Z.; Wang, S.; Jiao, L. Geochemical behavior of metals-sulfide-phosphorus at SWI (sediment/water interface) assessed by DGT (Diffusive gradients in thin films) probes. *J. Geochem. Explor.* **2015**, *156*, 145–152. [CrossRef]
26. Xu, D.; Wu, W.; Ding, S.; Sun, Q.; Zhang, C. A high-resolution dialysis technique for rapid determination of dissolved reactive phosphate and ferrous iron in pore water of sediments. *Sci. Total Environ.* **2012**, *421–422*, 245–252. [CrossRef] [PubMed]
27. Duan, H.; Ma, R.; Xu, X.; Kong, F.; Zhang, S.; Kong, W.; Hao, J.; Shang, L. Two-decade reconstruction of algal blooms in China's Lake Taihu. *Environ. Sci. Technol.* **2009**, *43*, 3522–3528. [CrossRef] [PubMed]
28. Qin, B.Q.; Xu, P.Z.; Wu, Q.L.; Luo, L.C.; Zhang, Y.L. Environmental issues of Lake Taihu, China. *Hydrobiologia* **2007**, *581*, 3–14. [CrossRef]
29. Xu, H.; McCarthy, M.J.; Paerl, H.W.; Brookes, J.D.; Zhu, G.; Hall, N.S.; Qin, B.; Zhang, Y.; Zhu, M.; Hampel, J.J.; et al. Contributions of external nutrient loading and internal cycling to cyanobacterial bloom dynamics in Lake Taihu, China: Implications for nutrient management. *Limnol. Oceanogr.* **2021**, *66*, 1492–1509. [CrossRef]
30. Xu, H.; Paerl, H.W.; Qin, B.; Zhu, G.; Hall, N.S.; Wu, Y. Determining Critical Nutrient Thresholds Needed to Control Harmful Cyanobacterial Blooms in Eutrophic Lake Taihu, China. *Environ. Sci. Technol.* **2015**, *49*, 1051–1059. [CrossRef] [PubMed]
31. Qin, B.; Paerl, H.W.; Brookes, J.D.; Liu, J.; Jeppesen, E.; Zhu, G.; Zhang, Y.; Xu, H.; Shi, K.; Deng, J. Why Lake Taihu continues to be plagued with cyanobacterial blooms through 10 years (2007–2017) efforts. *Sci. Bull.* **2019**, *64*, 354–356. [CrossRef] [PubMed]
32. Jiang, X.Y.; Gao, G.; Zhang, L.; Tang, X.M.; Shao, K.Q.; Hu, Y.; Cai, J. Role of algal accumulations on the partitioning between N_2 production and dissimilatory nitrate reduction to ammonium in eutrophic lakes. *Water Res.* **2020**, *183*, 116075. [CrossRef]
33. Peng, Y.; Liu, L.; Jiang, L.; Xiao, L. The roles of cyanobacterial bloom in nitrogen removal. *Sci. Total Environ.* **2017**, *609*, 297–303. [CrossRef] [PubMed]
34. Zhu, L.; Shi, W.; Zhou, J.; Yu, J.; Kong, L.; Qin, B. Strong turbulence accelerates sediment nitrification-denitrification for nitrogen loss in shallow lakes. *Sci. Total Environ.* **2021**, *761*, 143210. [CrossRef]
35. Yao, Y.; Li, D.; Chen, Y.; Han, X.; Wang, G.; Han, R. High-resolution characteristics and mechanisms of endogenous phosphorus migration and transformation impacted by algal blooms decomposition. *Sci. Total Environ.* **2022**, *820*, 152907. [CrossRef]
36. Ren, M.Y.; Ding, S.M.; Shi, D.; Zhong, Z.L.; Cao, J.X.; Yang, L.Y.; Tsang, D.C.W.; Wang, D.; Zhao, D.H.; Wang, Y. A new DGT technique comprised in a hybrid sensor for the simultaneous measurement of ammonium, nitrate, phosphorus and dissolved oxygen. *Sci. Total Environ.* **2020**, *725*, 11. [CrossRef]
37. Ding, S.; Chen, M.; Gong, M.; Fan, X.; Qin, B.; Xu, H.; Gao, S.; Jin, Z.; Tsang, D.C.W.; Zhang, C. Internal phosphorus loading from sediments causes seasonal nitrogen limitation for harmful algal blooms. *Sci. Total Environ.* **2018**, *625*, 872–884. [CrossRef]
38. Ding, S.M.; Han, C.; Wang, Y.P.; Yao, L.; Wang, Y.; Xu, D.; Sun, Q.; Williams, P.N.; Zhang, C.S. In situ, high-resolution imaging of labile phosphorus in sediments of a large eutrophic lake. *Water Res.* **2015**, *74*, 100–109. [CrossRef]
39. Yao, Y.; Han, X.; Chen, Y.; Li, D. The variations of labile arsenic diffusion driven by algal bloom decomposition in eutrophic lake ecosystems. *Sci. Total Environ.* **2022**, *842*, 156703. [CrossRef] [PubMed]
40. Chen, X.F.; Yang, L.Y.; Xiao, L.; Miao, A.J.; Xi, B.D. Nitrogen removal by denitrification during cyanobacterial bloom in Lake Taihu. *J. Freshw. Ecol.* **2012**, *27*, 243–258. [CrossRef]
41. Hou, J.; Song, C.; Cao, X.; Zhou, Y. Shifts between ammonia-oxidizing bacteria and archaea in relation to nitrification potential across trophic gradients in two large Chinese lakes (Lake Taihu and Lake Chaohu). *Water Res.* **2013**, *47*, 2285–2296. [CrossRef]
42. Sobek, S.; Gudasz, C.; Koehler, B.; Tranvik, L.J.; Bastviken, D.; Morales-Pineda, M. Temperature Dependence of Apparent Respiratory Quotients and Oxygen Penetration Depth in Contrasting Lake Sediments. *J. Geophys. Res. Biogeosci.* **2017**, *122*, 3076–3087. [CrossRef]
43. Bastviken, D.; Persson, L.; Odham, G.; Tranvik, L. Degradation of dissolved organic matter in oxic and anoxic lake water. *Limnol. Oceanogr.* **2004**, *49*, 109–116. [CrossRef]
44. Lambert, T.; Bouillon, S.; Darchambeau, F.; Morana, C.; Roland, F.A.E.; Descy, J.-P.; Borges, A.V. Effects of human land use on the terrestrial and aquatic sources of fluvial organic matter in a temperate river basin (The Meuse River, Belgium). *Biogeochemistry* **2017**, *136*, 191–211. [CrossRef]
45. Walker, S.A.; Amon, R.M.W.; Stedmon, C.A. Variations in high-latitude riverine fluorescent dissolved organic matter: A comparison of large Arctic rivers. *J. Geophys. Res. Biogeosci.* **2013**, *118*, 1689–1702. [CrossRef]
46. Lee, S.-A.; Kim, T.-H.; Kim, G. Tracing terrestrial versus marine sources of dissolved organic carbon in a coastal bay using stable carbon isotopes. *Biogeosciences* **2020**, *17*, 135–144. [CrossRef]
47. Ren, W.; Wu, X.; Ge, X.; Lin, G.; Zhou, M.; Long, Z.; Yu, X.; Tian, W. Characteristics of dissolved organic matter in lakes with different eutrophic levels in southeastern Hubei Province, China. *J. Oceanol. Limnol.* **2021**, *39*, 1256–1276. [CrossRef]
48. Catala, T.S.; Reche, I.; Fuentes-Lema, A.; Romera-Castillo, C.; Nieto-Cid, M.; Ortega-Retuerta, E.; Calvo, E.; Alvarez, M.; Marrase, C.; Stedmon, C.A.; et al. Turnover time of fluorescent dissolved organic matter in the dark global ocean. *Nat. Commun.* **2015**, *6*, 5986. [CrossRef]

49. Dainard, P.G.; Guéguen, C. Distribution of PARAFAC modeled CDOM components in the North Pacific Ocean, Bering, Chukchi and Beaufort Seas. *Mar. Chem.* **2013**, *157*, 216–223. [CrossRef]
50. Sharma, P.; Laor, Y.; Raviv, M.; Medina, S.; Saadi, I.; Krasnovsky, A.; Vager, M.; Levy, G.J.; Bar-Tal, A.; Borisover, M. Compositional characteristics of organic matter and its water-extractable components across a profile of organically managed soil. *Geoderma* **2017**, *286*, 73–82. [CrossRef]
51. Liu, C.; Du, Y.; Yin, H.; Fan, C.; Chen, K.; Zhong, J.; Gu, X. Exchanges of nitrogen and phosphorus across the sediment-water interface influenced by the external suspended particulate matter and the residual matter after dredging. *Environ. Pollut.* **2019**, *246*, 207–216. [CrossRef]
52. Lu, K.; Gao, H.; Yu, H.; Liu, D.; Zhu, N.; Wan, K. Insight into variations of DOM fractions in different latitudinal rural black-odor waterbodies of eastern China using fluorescence spectroscopy coupled with structure equation model. *Sci. Total Environ.* **2022**, *816*, 151531. [CrossRef] [PubMed]
53. Retelletti Brogi, S.; Ha, S.Y.; Kim, K.; Derrien, M.; Lee, Y.K.; Hur, J. Optical and molecular characterization of dissolved organic matter (DOM) in the Arctic ice core and the underlying seawater (Cambridge Bay, Canada): Implication for increased autochthonous DOM during ice melting. *Sci. Total Environ.* **2018**, *627*, 802–811. [CrossRef] [PubMed]
54. Bao, Y.; Huang, T.; Ning, C.; Sun, T.; Tao, P.; Wang, J.; Sun, Q. Changes of DOM and its correlation with internal nutrient release during cyanobacterial growth and decline in Lake Chaohu, China. *J. Environ. Sci.* **2023**, *124*, 769–781. [CrossRef]
55. Zhu, L.; Shi, W.; Van Dam, B.; Kong, L.; Yu, J.; Qin, B. Algal Accumulation Decreases Sediment Nitrogen Removal by Uncoupling Nitrification-Denitrification in Shallow Eutrophic Lakes. *Environ. Sci. Technol.* **2020**, *54*, 6194–6201. [CrossRef]
56. Shi, K.; Zhang, Y.L.; Zhang, Y.B.; Li, N.; Qin, B.Q.; Zhu, G.W.; Zhou, Y.Q. Phenology of Phytoplankton Blooms in a Trophic Lake Observed from Long-Term MODIS Data. *Environ. Sci. Technol.* **2019**, *53*, 2324–2331. [CrossRef] [PubMed]
57. Poulson, S.R.; Sullivan, A.B. Assessment of diel chemical and isotopic techniques to investigate biogeochemical cycles in the upper Klamath River, Oregon, USA. *Chem. Geol.* **2010**, *269*, 3–11. [CrossRef]
58. Zhang, H.; Davison, W. Performance characteristics of diffusion gradients in thin films for the in situ measurement of trace metals in aqueous solution. *Anal. Chem.* **1995**, *67*, 3391–3400. [CrossRef]
59. Sun, Q.; Chen, J.; Zhang, H.; Ding, S.M.; Li, Z.; Williams, P.N.; Cheng, H.; Han, C.; Wu, L.H.; Zhang, C.S. Improved diffusive gradients in thin films (DGT) measurement of total dissolved inorganic Arsenic in waters and soils using a hydrous zirconium oxide binding layer. *Anal. Chem.* **2014**, *86*, 3060–3067. [CrossRef]
60. Xu, D.; Ding, S.M.; Sun, Q.; Zhong, J.C.; Wu, W.; Jia, F. Evaluation of in situ capping with clean soils to control phosphate release from sediments. *Sci. Total Environ.* **2012**, *438*, 334–341. [CrossRef]
61. Gao, Y.; Lesven, L.; Gillan, D.; Sabbe, K.; Billon, G.; De Galan, S.; Elskens, M.; Baeyens, W.; Leermakers, M. Geochemical behavior of trace elements in sub-tidal marine sediments of the Belgian coast. *Mar. Chem.* **2009**, *117*, 88–96. [CrossRef]
62. Krausfeldt, L.E.; Tang, X.; van de Kamp, J.; Gao, G.; Bodrossy, L.; Boyer, G.L.; Wilhelm, S.W. Spatial and temporal variability in the nitrogen cyclers of hypereutrophic Lake Taihu. *FEMS Microbiol. Ecol.* **2017**, *93*, fix024. [CrossRef] [PubMed]